International Journal of Scientific & Engineering Research, Volume 5, Issue 12, December-2014
ISSN 2229-5518

Lung Nodule Segmentation based on Modified Local Binary Pattern

Sarah Soltaninejad, Mohammad Hosein Shakoor, Farshad Tajeripour

Abstract— In this paper a new CAD system is proposed for segmentation of lung nodules in CT images which calculate volume of them. For lung segmentation, a new idea is proposed based on the concavity degree of border points that solves nodule problem which is attached to the chest wall. In nodule detection, two important steps are followed: feature extraction and classification. For feature extraction, some texture features are extracted based on an extended type of Local Binary Pattern. LBP is one of the most important feature extractor in texture image but it is more sensitive to noise. Support Vector Machine (SVM) is used for classification to distinct the pathological change (nodule) from other normal regions of the chest. After detection of (rectangular) region of a nodule, because of the similarity between the intensity of nodules and some background parts such as vessels using traditional threshold cannot exclude these backgrounds accurately. In this paper, a new method is proposed that uses uniform texture information to overcome this problem. After extraction of nodule contour, the volume of each nodule is calculated precisely.

Index Terms— Local binary pattern (LBP), Nodule detection, Lung segmentation, Concavity degree, Nodule volumetric.

1. INTRODUCTION

LONG Lung cancer is the most common cause of cancer deaths in the world. In the last few years, many computer-aided detection (CAD) systems have been proposed to help radiologists to diagnose diseases such as automatic detection of lung nodules in CT scans [1]. These systems make it possible to detect diseases very faster than a specialist alone. Recent research has demonstrated the advantages of using CAD systems to help physicians in the detection [2-4] and diagnosis of lung cancer [8]. A CAD system for CT images includes three important parts: 1) preprocessing and lung segmentation, 2) features extraction part that extracts features of each sub-region of CT image by using some descriptors and 3) A classifier that divides sub-regions of CT images into normal and abnormal (nodule).

At the beginning of the algorithm some prepossessing operations must be applied on each CT image. Then lung curve should be extracted to exclude all redundant parts from each CT image [5-9]. Also there are many features that can be used for classification. The texture features are fundamental features for image segmentation [10, 11], image classification [12, 13], image retrieval systems [14, 15], etc. In the past 10 years, some methods based on the texture features were proposed. These methods such as the gray level difference method (GLDM), the gray level run-length method (GLRLM), and the spatial gray level dependent method (SGLDM) [16] have been widely used to extract medical image characteristics and structures that are not directly visible for observers.

There are some automatic methods for lung nodule detection. Most of these methods use segmentation before classification in lung image to extract nodules of image. Ozekes [17] used a segmentation algorithm based on rules and template matching trained with genetic algorithm (GA) which achieved 93.4% sensitivity and 0.59% false positives per exam. Ozekes et al. [18] achieved 100% sensitivity and a rate of 13.37% false genetic neural network and threshold based on fuzzy rules. In [19], Ye et al. used a set of different features, containing intensity information, shape index, and 3D spatial location for nodule detection. Antonelli et al. [20], used fuzzy c-means, followed by a morphological analysis of the resulting structures for this purpose. The automatic detection of low-dose CT images (LDCT) was reported in [21] using information from probabilistic models created to control the evolution of a deformable model, that was able to segment the lung nodules with low average error and low standard deviation with respect to the form described by the specialist. In [22] Messay et al. combined simple image processing techniques, such as intensity thresholding and morphological operations, to segment and detect structures that were lung nodule candidates. The authors did feature selection among 245 features to determine the lung nodule candidates and used them in two classifiers: the Fisher Linear Discriminant classifier and a quadratic classifier. The method was able to detect 92.8% of the structures, which were nodule candidates. The CAD system proposed by Tan et al. [23] employed three classifiers; one of them is based on genetic algorithms and artificial neural networks, which are then, compared to results from SVM and fixed-topology neural networks. The lung nodule detection method includes filters to detect nodules and vessels, and divergence features to locate possible lung nodule candidates. Once the candidates are detected, features in a gauge system are

applied to the three classifiers. The results obtained with the fixed-topology neural network had sensitivity of 87.5%, with average of four false positives per exam for nodules with diameter larger than or equal to 3 mm. Opfer et al. [24] have shown how to evaluate the performance of CAD systems using a standard dataset, which has the ground truth given by four specialists. In their analyses, the authors showed that their CAD system is able to reach detection rate of 89% of the lung nodules. Because of some special texture of nodule of CT images, texture features are widely used for nodule detection. One of the most important descriptors that can provide feature of texture accurately is Local Binary Pattern (LBP) [25]. LBP is a powerful texture descriptor that is widely used in various applications to extract some texture features. The 2 riuLBP [26] is rotation invariant LBP by using the uniform local pattern. To further benefit from the uniform local pattern is extended LBP (ELBP) that can be used as a good measure of an image's uniformity. In most paper each segmented lung is divided into some sub-regions and for each sub-region, texture features are extracted from the co-occurrence matrix. The co-occurrence matrix is made based on ELBP and Gradient of Difference (GOD) of each point. Then the features of each sub-region are fed into Support Vector Machine (SVM) to classify each sub-region into nodule and normal region. Segmentation of nodule in CT images is hard because there are many interviewing parts in the images, such as location and structure of the nodules, and the presence of neighbor structures with similar densities such as nodule. Also similar intensity and direct connection of nodules to other resembling parts, complicate nodule contour extraction. The proposed segmentation uses LBP for excluding background of detected sub-region from its nodule part. This new proposed method uses Threshold LBP (TLBP). In this part LBP (TLBP) is not used for texture features extraction, but it is used for thresholding to exclude background of nodule. The gray level image of TLBP (GTLBP) is made by TLBP information. If GTLBP is used as gray scale image, the intensity of pixels in GTLBP has discrimination information in nodule parts, which is used for segmenting nodule in detected sub-region. This method is proposed to remove vessel and other parts with similar intensity that connected to the nodules.

After nodule segmentation, it is possible to calculate volume of each nodule. Volume measurement is usually based on segmentation of nodules in thin-section CT data sets. Some computer-based algorithms use Multi Detector CT (MDCT) chest scans (special type of CT scan) involve automatic detection and measurements of the nodules. Various studies have shown that volume measurement of pulmonary nodules is reliably possible [27]-[29]. However, there are only a few studies on the follow-up examinations of metastatic nodules during chemotherapy, using volume measurement from CT to precisely analyze a subject response to treatment. The current study has many advantages. For example it can be used to compare the manual measurements (diameter, area, and attenuation) to the automatic volumetric assessment of lung metastases during chemotherapy. Also it is useful for evaluating the changes in attenuation of metastases and its influence on interpretation of the follow-up examinations. On the other hand, evaluations of volume of nodule have been reported to be helpful in differentiating between benign and malignant nodules [30]-[33]. The growth rate can then easily be derived from comparing volume measurements. Furthermore, in an oncologic setting, volume measurements can be very useful to assess the response of metastatic lung lesions to chemotherapy. There are many methods for monitoring nodules. One of the standards for monitoring solid nodules is known as RECIST (response evaluation criteria in solid tumors) [34]-[36]. RECIST is a latent standard for assessing diseases progression (or regression) in patients with lung cancer [34]. However, the RECIST measurement standard is limited to the longest, in-plane diameter of a tumor as a proxy for tumor size and is thought to be potentially problematic because tumors do not always expand or contract uniformly [36]. A solution to the limitations of RECIST may be the use of volume measurement tools [37]. In spite of conducting research to improve nodule detection, in this paper, we develop a method to measure the volume of detected nodules. In other words, our objective is to propose an automatic system which not only detects the nodule sub-region but also extracts contour of nodule precisely and then calculates its volume accurately.

This paper is organized as follows: Section 2 presents block diagram of system and preprocessing and our method for lung segmentation, Section 3 describes feature extraction method and nodule detection and in section 4 nodule segmentation and volumetric are proposed. Experimental results and conclusion are shown in sections 5 and 6, respectively.

This paper is organized as follows: Section 2 presents our CAD system, Section 3 describes feature extraction method and proposed method, experimental results and conclusion are shown in sections 4 and 5, respectively.

2. PROPOSED METHOD

In this paper, a CAD system for pulmonary nodule segmentation and volumetric is proposed. The proposed system includes three basic parts.

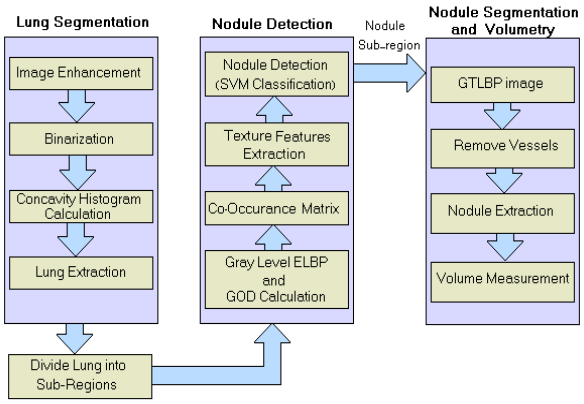

Fig. 1: Block diagram of proposed method.

Fig.1 shows these parts in detail. Lung segmentation includes some preprocessing operations and segmentation process which is based on the concavity degree of border points. The next step of CAD system is nodule detection that follows two steps: feature extraction and classification. In the proposed method, texture features are extracted based on a threshold ELBP method and classification is applied by SVM classifier. A new idea is proposed for removing vessel parts in nodule sub-region candidate which consider as nodule part. This step that used for nodule segmentation causes false positive reduction in nodule segmentation part. Finally the volume of nodule is calculated.

2.1. Lung *Segmentation*

The first step in every CAD system is lung segmentation for minimizing the search space for nodule detection and cause to have a faster system. In the lung segmentation step, it is necessary to enhance CT images and remove some redundant region of the images. Noises are removed by median filter because this filter has high noise removing ability and low blurring effect comparison with other filters [38]. Furthermore, these characteristics can be controlled by setting appropriate size for the filter window. Then, images are enhanced by gamma correction. Fig.2a-2c represents original image, denoised image and enhanced image. After image enhancement, it is necessary to extract lung parts from other parts. Firstly, a binary image is obtained by Otsu method [39] and the border of the lung region in each slice is extracted by canny edge detection method. Fig.2f-2g shows that some nodules that attach to chest wall are removed but the lung segmentation process should consider these nodules as lung parts to segment them in nodule detection part. In this paper, a novel method is proposed that solves this problem by using the concavity degree of border points. In the proposed method, first the lung borders are traced in a sequence of n pixels, so they form a collection of directed closed contours defined in (1) and extra contours are removed based on the number of pixels in each contour. Fig.2d-2g represents results of these steps.

$$Lung\ border = \{L_i \mid (p_1, p_2, .., p_{n_i}), i \in [1, m]\} \quad (1)$$

In equation (1) m is the number of the directed loops forming the lung border, L_i is the i^{th}direction loop of the lung border and p is a pixel of the lung border. Second, the concavity degree of each pixel in the remaining contours will be computed. Angles and curvature are widely used for concavity calculation. However, both angle and curvature are vulnerable to noise, especially when the segmentation step cannot produce a neat and clean contour because of the noise. The property of the convex regions is used to define a new concavity calculation method that was used for computing the centerline of the chromosome by Mohamadi [49]. Fig.3 shows the convex hull region property in an image. Based on the above discussion, for the concave points, the straight line segment between two near boundary points is outside of the region. This property is shown in Fig.2.

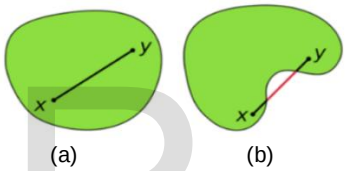

Fig. 3: Demonstration of convex hull and non-convex hull, a) Convex, b) Non-convex (concave).

Concavity degree computation of each boundary pixel corresponds to boundary points by distance h that are considered as two endpoints of the base line. The base line determines the type of point (convex or concave). Thus, this base line is plotted and its points that are not on the region are counted. The concavity degree defines as the ratio of the number of outside points toward the base line and the total number of the line segment points.

$$C_i = \frac{\sum L_i \cap R'}{\sum L_i} \quad (2)$$

Equation (2) shows this ratio where R is the region of the lung and R' is its complement. Also, L_i is the region of the line segment and C_i is the concavity degree corresponding to the i^{th} boundary pixel. Moreover, operator $\sum$ calculate the number of non-zero values in the corresponding operand. Thus, the value of $\sum L_i$ is equal to 2h-1 (two endpoints are not counted as the line segment points). The resulted image of assigning concavity degree to the boundary points is called "concave image". In the concave image, we have lower intensity in border points where they are in non-convex parts but in other parts of the contour,

the intensity is high. Third, after computing concavity degree of boundary points of the lung, the histogram of these degrees is drawn related to pixels belong to the borders. Fig.6.a shows this histogram curve for the first lung border of our current slice. Then, we apply Gaussian filter for removing noise and weak local maximums which is represented in Fig.6.b. Finally, every pair of strong local maxima is obtained. If Euclidean distance between each pair of point is lower than a pre-defined threshold distance, these points indicate a hole on the border and the edge between them was replaced by a straight line otherwise main edge is kept. In Fig.5.b an example of this pair of points is shown and the local maxima of it, is illustrated in Fig5.d. After closing all holes on the edge of each contour, the border mask is obtained. Fig.6.a shows a complete contour. After that, we can apply extracted border as a mask on the original image and retrieve lung regions. Fig.6.b shows extracted lung from the original CT image.

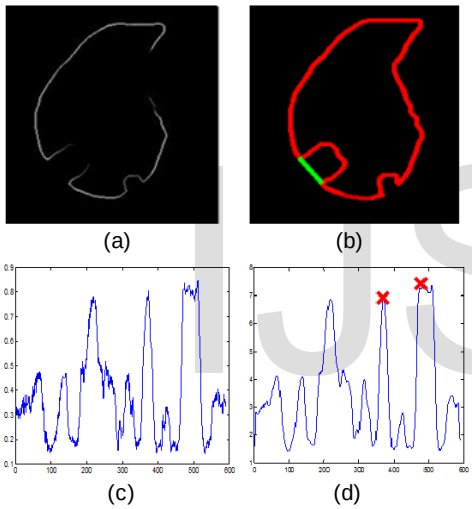

Fig. 5: a) Current contour, b) closed holes of determined points c) Contour histogram, d) Clean concavity histogram (A pair of point indicate hole on the border).

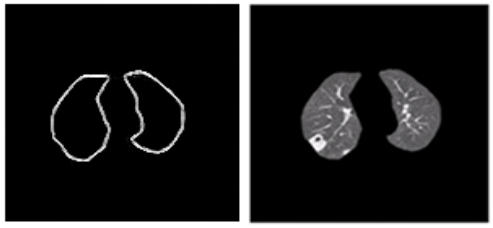

Fig. 6: Result of lung segmentation: a) Lung contour; b) Extracted lung.

2.2. Nodule Detection

After lung segmentation step in a CAD system, we can detect nodules by classifying the pixels located in the segmented lung area into two classes: nodule and non-nodule. This step contains two parts that are described below: feature extraction and classification. Texture features are obtaining and SVM classifier is used for classification.

2.2.1. Feature Extraction and Classification

In any classification task, feature extraction is very important because extracting discriminant features cause to better data separation and higher classification rate [10]. To extract the texture features from the lung and recognize nodule regions, each image is separated into sub-regions as Liang, Tanaka and Nakamura [22] did. Fig.3a and Fig.3b show the sub-regions of a lung image for small and large sub-region respectively. Value of d (dimension of square sub-region) must be selected properly. If it is so large, it may decrease accuracy of classification. On the other hand, using very small sub-regions increases the number of train and test data and results in high computational complexity for train and test operations. Therefore, d should be set same as the size of diameter of medium nodules. For nodule detection it is possible to use large sub-region to determine only the sub-region (location) of each nodule. All sub-regions are not used for feature extraction, because there are some only black or only white sub-regions that do not have any information. In Fig.3a and Fig.3b these parts are white or black completely. For each sub-region, the Extended LBP values are mixed with gradient difference to make co-occurrence matrix which is used to extract some features for classification.

Nodules in the CT images have especial texture structure. In order to make distinction between nodules and the normal regions, some features are required. For this purpose, Penget proposed the uniformity estimation method (UEM) [29] based on local binary pattern (LBP), which can extract the uniformity information of brightness and structure in multiple directions from lung image. In order to extract texture features in multiple directions, we propose a modified extension of rotation invariant local binary pattern that uses a threshold value. At first LBP is introduced.

2.2.2. Local Binary Pattern (LBP)

The LBP [34] is a powerful tool for describing texture features and has been widely used in a large number of applications such as face recognition [52] and medical image analysis [53]. The first LBP operator, which was introduced in [34], generates binary codes by comparing points of the for example 3*3 neighboring pixels with respect to the center pixel value. It generates a binary code 0 if the value of neighbor pixel is smaller than that of the center pixel. Otherwise, it generates a binary code 1. Then the binary codes are multiplied with the corresponding weights and the results are summed up to generate an LBP code. This value is calculated as follow in Equation (3):

$$LBP_{P,R}(x,y)=\sum_{i=0}^{P-1}s(g_i-g_c)2^i \quad (3)$$

$$s(g_i-g_c)=\begin{cases}1 & g_i \geq g_c \\ 0 & else\end{cases} \quad (4)$$

Where g_c is the pixel value of the center point and g_i is the pixel value of the neighboring pixel, P is the number of neighbor pixels, R is the radius.

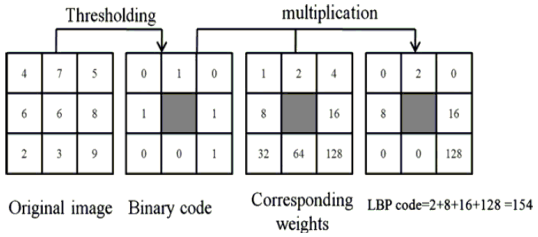

Fig. 8: The process of calculating the LBP code.

Fig. 8 shows the process of generating LBP code. . At last, each LBP code is used as a feature value. Also it can be used in a LBP histogram. Each bin of LBP histogram shows the number of a LBP code value. There are many versions of LBP that extract texture feature of image. Most of these methods are not rotate invariant. To obtain rotation invariance, the original LBP was then extended to a circular symmetric neighbor set of P members on a circular region with radius R using uniform patterns [35].The rotation invariance LBP (LBP^{riu2}) can be obtained as follows (Equations. (5)-(7)).

$$LBP_{P,R}^{riu2}(x,y)=\begin{cases}\sum_{i=0}^{P-1}s(g_i-g_c) & if\ U(LBP_{P,R})\le 2\\ P+1 & else\end{cases} \quad (5)$$

$$s(g_i-g_c)=\begin{cases}1 & if\ g_i\ge g_c\\ 0 & else\end{cases} \quad (6)$$

$$U(LBP_{P,R})=|\,s(g_{p-1}-g_c)-s(g_0-g_{c})\,|+\sum_{i=1}^{P}|\,s(g_i-g_c)-s(g_{i-1}-g_{c})\,| \quad (7)$$

Here, riu2 reflects that the rotation invariant uniform patterns have a U value of at most 2. U is used to estimate the uniformity that corresponds to the number of spatial transitions, i.e., bitwise 0/1 changes between successive bits in the circle. Fig.9 is an example of the local uniform pattern with different U.

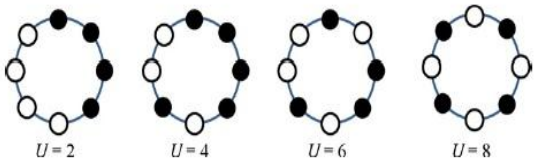

Fig. 9: An example of local binary patterns with different U.

LBP^{riu2} is rotation invariant method and merges rotated features and produces only P+1 features rather that P^2features of LBP. LBP^{riu2} uses uniform local pattern by using U<=2.To further describe the brightness uniformity of the local patterns and make the LBP more distinctive, Uniformity Estimation Method (UEM) [50] used $ELBP^{riu4}$ by redefining Equations (5)-(7) as Equations (8)-(11).

$$ELBP_{P,R}^{riu4}(x,y)=\begin{cases}\sum_{i=0}^{P-1}|\,s(g_i-g_c)\,| & if\ U(ELBP_{P,R})\le 4\\ P+1 & else\end{cases} \quad (8)$$

Where

$$s(g_i-g_c)=\begin{cases}1 & g_i>g_c\\ 0 & g_i=g_c\\ -1 & g_i<g_c\end{cases} \quad (9)$$

$$U(ELBP_{P,R})=d(s(g_{p-1}-g_c)-s(g_0-g_c))+\sum_{i=1}^{P}d(s(g_i-g_c)-s(g_{i-1}-g_c)) \quad (10)$$

$$d(x)=\begin{cases}0 & x=0\\ 1 & else\end{cases} \quad (11)$$

2.2.3. Proposed ELBP (TELBP)

As we can see from (9), the brightness relationship between the center point and its neighboring pixels is divided into three situations that are given by different labels (-1, 0, and 1). This new pattern can distinguish the brightness relationship between the center point and its neighboring pixels in more details. But it is more sensitive to noise rather than LBP. We proposed new method of ELBP which is named TELBP that uses threshold parameter T. This new method is more robust to noise and obtain information in multiple directions which is shown as bellow Equation (12). So $TELBP^{riu4}$ is the same as $ELBP^{riu4}$ and only difference is shown in Equation (12) instead of Eq.(5) and using U<=2 instead of U<=4. Also if CT images do not have noise, we must set T=0. If T=0, Equation (12) is the same as Equation (9). By setting T properly, the ELBP is more robust to noise and produces better discrimination information than T=0. In our implementation value of T depends on the variance of noise in CT image (after preprocessing) the more variance of noise the greater value of T. If R=1 in LBP^{riu2}, more than 90 percent of local pattern is uniform pattern. For R>1 this percentage decrease slightly (around 20 percent for R=2 and etc.). Therefore, it can be used to determine X value in (12). X must be set to 1 or 0 to produce uniform pattern. LBP^{riu2} uses uniform local binary pattern by using U<=2. So each undetermined bit in (12) must set to 0 or 1 to produce uniform pattern.

$$d(g_i-g_c)=\begin{cases}1 & g_i>g_c+T\\ 0 & g_c-T\le g_i\le g_c+T\\ -1 & g_i<g_c-T\end{cases} \quad (12)$$

2.2.4. Local structure using gradient orientation difference

To describe the local structures, [41] proposed to apply the gradient orientations of the points. The gradient orientation is another good measure of representation of the image features [45]-[46]. The image intensity function is I (x, y). The gradient orientation of point P(x, y) is calculated as follows based on the Sobel mask as Equation (13).

$$\theta(x,y) = \arctan\left(\frac{I(x,y+1)-I(x,y)}{I(x+1,y)-I(x,y)}\right) \quad (13)$$

Therefore, given a point P(x,y) and its neighboring point $P(x_n, y_n)$, the gradient orientation differences between P(x,y) and all neighbor points (n=1 to P=8) are obtained by (14).

$$GOD(x,y)_{x_n,y_n} = |\theta(x,y) - \theta(x_n,y_n)| \quad n = 1,..,P = 8 \quad (14)$$

In this equation GODs of all 8 neighbor points are calculated and all of these 8 values are applied in co-occurrence matrix in Equation (16).

$$\begin{cases} GLELBP^{riu4}(x,y) = g_c * \dfrac{TELBP^{riu4}_{P,R}(x,y)}{P+1} \\ GOD(x,y)_{x_n,y_n} = |\theta(x,y) - \theta(x_n,y_n)| \quad ; n = 1,..,P = 8 \end{cases} \quad (15)$$

2.2.5. Texture Features Extraction

Now, for a point P (x, y), the $ELBP^{riu4}$ is employed to denote the brightness uniformity of the neighbors of P (x, y) and the gradient orientation difference that is applied to denote the local structural uniformity among P (x, y) and its neighbors. Suppose the number of neighboring points is P, defined radius is R, and neighboring points are $P(x_1, y_1),...,P(x_P, y_P)$ a pair of uniformity based values is defined between a given point P (x, y) and its neighbor point $P(x_n, y_n)$ based on Equation (15) where g_c is the gray level of P (x, y). Similarly, the pairs of uniformity based values for P(x, y) and $P(x_1, y_1),...,P(x_8, y_8)$ (for P=8 neighbor points) can be obtained by Equation (15). As we can see in Equation (15), the $GLELBP^{riu4}$ is the gray level based $TELBP^{riu4}$, which is a combination of the gray level and the $TELBP^{riu4}$. The gray level is degraded by the $TELBP^{riu4}$. Thus, if the points around P(x, y) are uniform will obtain a lower value or vice versa. Finally, the bright and structural uniformity can be estimated by applying Equation (15). According to this equation, a conditional probability density function F($GLELBP^{riu4}$;GOD|P,R) can be defined based on Equation(16), where $0 \le GLELBP^{riu4} \le L$ (suppose the gray level range is [0, L]), and 0≤GOD≤D (suppose the range of the degrees of gradient orientation difference is [0,D]). Finally, a co-occurrence matrix with the size of (L+1)*(D+1) can be used for making probability matrix as Equation (16).

$$UEM(GLELBP^{riu4}, GOD|P,R) = \begin{bmatrix} F(0,0|P,R) & F(0,1|P,R) & \cdots & F(0,D|P,R) \\ F(1,0|P,R) & F(1,1|P,R) & \cdots & F(1,D|P,R) \\ \vdots & \vdots & \vdots & \vdots \\ F(L,0|P,R) & F(L,1|P,R) & \cdots & F(L,D|P,R) \end{bmatrix} \quad (16)$$

F (l, d | P, R) value is probably of gray scale l and gradient difference d in $GLELBP^{riu4}$ image. For each l value there are P values of d because of P neighbor points. So, all of these P pair values must be applied to co-occurrence matrix. Then some texture features are extracted from this matrix as Equations. (17-23).

1) Entropy:

$$ENT = -\sum_{l=0}^{L}\sum_{d=0}^{D} F(l,d|P,R)\log(F(l,d|P,R)) \quad (17)$$

2) Gradient Orientation Uniformity (GOU):

$$GOU = \sum_{l=0}^{L}\sum_{d=0}^{D} F(l,d|P,R)\,Cos(d) \quad (18)$$

3) Gradient Orientation Difference (GOD):

$$GOD = \sum_{l=0}^{L}\sum_{d=0}^{D} F(l,d|P,R)\,Sin(d/2) \quad (19)$$

4) High Gray Level:

$$HGL = \sum_{l=0}^{L}\sum_{d=0}^{D} F(l,d|P,R)\,l^2 \quad (20)$$

5) Homogeneity:

$$HMG = \sum_{l=0}^{L}\sum_{d=0}^{D} \frac{F(l,d|P,R)}{1+l^2} \quad (21)$$

6) Moment:

$$MMT = \sum_{l=0}^{L}\sum_{d=0}^{D} \frac{F(l,d|P,R)^2}{1+l^2} \quad (22)$$

7) Energy:

$$ENG = \sum_{l=0}^{L}\sum_{d=0}^{D} F(l,d|P,R)^2 \quad (23)$$

In these seven features, entropy is an indication of the complexity within an image; a complex image produces a high entropy value [26]. Orientation difference is a measure of the image structure difference. If the local structures of an image are different from each other, Gradient Orientation difference is high and Gradient Orientation Uniformity is low. High Gray Level value and Homogeneity are two measures of the image brightness. If

the image is bright, High Gray Level will achieve a high value and homogeneity obtains low value. The homogeneity is a measure of the structural uniformity of an image. It obtains a high value if the image is uniform, and vice versa. Also, Moment and Energy are two important features that are used to describe intensity of images. These 7 features are calculated for each sample (each sub-region of each segmented lung) and used by SVM for classification

2.3. Nodule Segmentation

In the proposed system next step is nodule segmentation and computing their volumes. In most of the papers, LBP is a way to extract texture information. Extended LBP is used in previous part to extract texture features of nodules and used them for classification. But, in this part a type of LBP is used for thresholding and masking on the detected nodule images. When the detected sub-region is determined by SVM it is possible to highlight this sub-region as a detected nodule. But it is not possible to determine volume of nodule because of some vessels and background tissues. Some thresholding methods can be used to extract nodule from its background, but in all of these methods it is very hard to exclude nodule from vessels because in most of lung area the intensity of nodule and vessel is the same and it is impossible to use traditional threshold method for this purpose. Two ways can be used for solving this problem. The first one is using small sub-regions instead of large sub-regions then using traditional threshold method to segment nodule. This method extracts small area of detected nodule precisely. Because the greatest part of each detected area includes nodule and the background parts such as vessels are very small and negligible but this method has two disadvantages; firstly, using small sub-region increases computation time significantly (especially in train and test part of SVM).Furthermore, it is not efficient for small nodule because for small nodules, this method makes difficult to calculate nodule volume accurately. The second, method is a new technique of thresholding that is proposed in this paper. This method is based on using threshold in gray level TLBP. Here GLELBP (Equation (15)) image is only used to calculate T for TLBP. The best T value in TLBP is related to difference of the intensity of vessel and nodule part in GLELBP image (not in the original image). The most important problem to exclude background of each sub-region is related to vessels. In this part rotate invariant LBP is used with threshold T and it is named TLBP. This method is not introduced to extract feature from nodule texture but it is used to segment nodule from its background. Equations of TLBP are the same as ELBP. Only difference is mentioned in Equation (24) (instead of Equation (9)). Other relations are the same as Equations.(8-10).

$$s(g_i - g_c) = \begin{cases} 1 & g_i \geq g_c + T \\ 0 & else \end{cases} \quad (24)$$

It is possible to show TLBP value as an image by Gray Level TLBP (GTLBP). GTLBP is based on Equation (15), if $TLBP^{riu4}$ is used instead of $ELBP^{riu4}$. GTLBP image is used for excluding vessel and elements which have similar intensity to nodule. Fig.10 shows GLELBP and GTLBP with various T (in all images P=8 and R=1). If the simple thresholding apply to GTLBP (not original image) it is possible to exclude vessels and others elements that have similar intensity to nodules from detected nodule sub-region. The aim of TLBP is to remove vessels from nodule detected sub-region and decreasing false positive value for nodule detection. All of recent explanation is defined in proposed nodule segmentation section. Fig.11 shows proposed steps. It is important to set T value precisely. The greater value of T the fewer vessels parts are excluded and vice versa. Also, if T is very small some parts of nodule may be deleted such as Fig.12.a. Increasing the T value has a limit and after that, it has not significant effect on image.

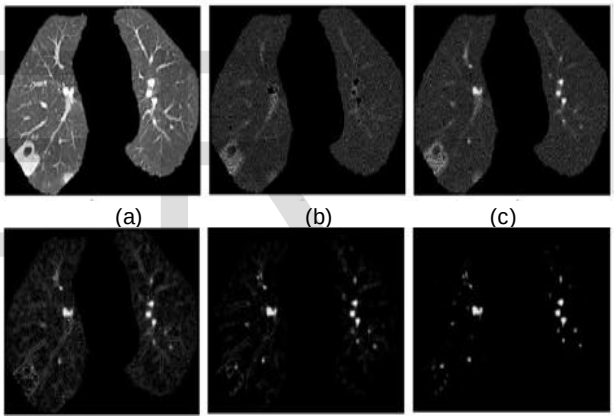

Fig. 10: Images with different parameters (P, R and T); a) Original image; b) GLELBP, P=8, R=1; c) GTLBP,P=8, R=1, T=0; d) GTLBP, P=8, R=1, T=20); e)GTLBP, P=8, R=1, T=40; f)GTLBP, P=8, R=1, T=100.

After obtaining GTLBP image some post processing should be done on the resulted image for obtaining the best mask to nodule segmentation. Some morphological operation (erosion by small disk structure element to remove very small points) apply on the resulted image and after that by using a simple threshold method, vessels will be extracted. Then, some other morphological operations are applied again and finally negative form of the last image used as a mask and applies to sub-region to remove vessels. Fig.11 shows these steps. It should be note that the method is applied for each detected nodule sub-region, but in this figures it is applied to entire of image to show its effect on all parts of the image.

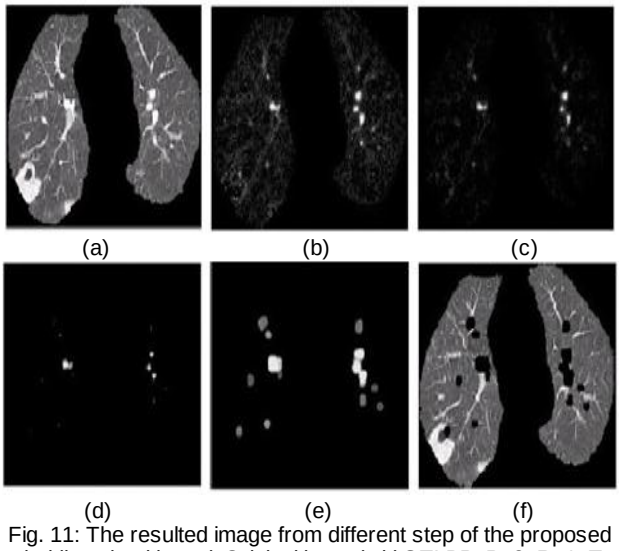

Fig. 11: The resulted image from different step of the proposed thresholding algorithm. a) Original image); b)GTLBP, P=8, R=1, T=10; c) Eroded image; d) Simple threshold image; e) Dilated image; f) Mask threshold GTLBP, P=8, R=1, T=10.

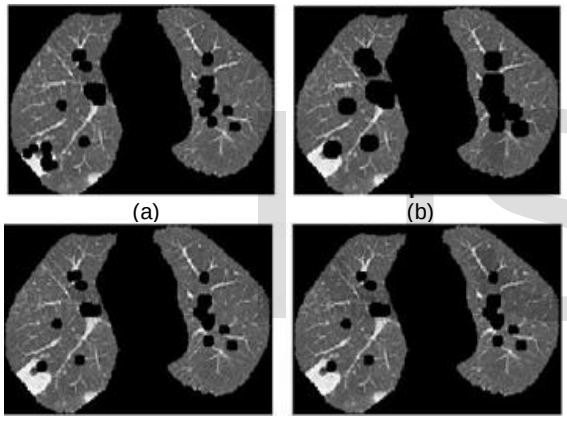

Fig. 12: Illustration of importance of choosing T: a) Mask threshold GTLBP, P=8, R=1, T=1; b) Mask threshold GTLBP,P=8, R=1, T=10; c) Mask threshold GTLBP, P=8, R=1,T=50; d) Mask threshold GTLBP, P=8, R=1, T=100.

2.4. Volume Measurement

After extraction of each nodule from each slice of CT image, the volume of detected nodule is computed by summing the volumes in each individual voxel that contains the tumor. There are some methods to calculate volume of each shape [48], each partially filled voxel geometry is computed based on a linear interpolation within that voxel. So, volume of each detected nodule can be fund for every patient as Equation (25):

$$NoduleVolume = \sum_{i=1}^{k} NoduleArea_i * SliceThickness \quad (25)$$

Where k is the number of slices and "Nodule Area" is the detected sub-region of nodule in 2D slices that was computed in previous step and the Thickness is a constant for special CT protocol.

3. EXPERIMENTAL RESULTS

In this section, results of the proposed method are presented and compared with some high performance algorithms. In the experimental results, eight clinical data sets with 19 nodules approved by medical experts are used. There are 45 slices/scans among which four data sets are 5 mm thickness. Also, there are 11 solid and two non-solid nodules in these data sets. Here, we have seven lung wall attached, one bronchiole attached and five solitary nodules. Another four data sets include about 450 slices/scans. There are four solid and two cavity nodules in these images. Four of these nodules are lung wall attached, one of them is bronchiole attached and the other one is solitary. These data sets were obtained in TABA medical imaging center of Shiraz medical school. Also Some CT images of LIDC dataset are used in train and test part [49].

Lung segmentation method that is proposed in this paper based on concavity degree can be compared with some other lung segmentation methods. There are some lung segmentation methods based on rolling ball and morphological operation such as [5] and [6] that are depend on radius of the ball and size of window but our proposed method is independent from this values. So, we propose a good method that extracted lung accurately that caused better results for the next steps. In the nodule detection, by using SVM classifier, the results of nodule detection have compared with some other methods. In this part by using TELBP instead of ELBP the accuracy of proposed method is increased and compared with three SGLDM, GLRLM, and GLDM [16]. These three methods are not rotate invariant but our method is rotate invariant. Also our proposed method is compared with UEM [41]. UEM is a well-known and rotate invariant method. Finally, the main motivation of this paper is related to volume measurement that used a proposed TLBP method for thresholding to exclude background of detected sub-region from nodule. The aim of this threshold method is related to false positive reduction in nodule segmentation. For feature extraction, image can divided into small or large such as Fig. 7 and for each sub-region texture features and GOD values are extracted and used in co-occurrence matrix. LibSVM [50] classifier is used for train and test. 70% of images are used for train and 30% for test. We evaluated the performances of proposed method for nodule detection according to the Sensitivity, Specificity, and Accuracy that are related to True Positive, True Negative, False Positive, and False Negative as follows:

- True positive (TP): the number of abnormal sub-regions that are correctly classified.
- True negative (TN): the number of normal sub-regions that are correctly classified.

- False positive (FP): the number of normal sub-regions that are incorrectly classified as abnormal regions.
- False negative (FN): the number of abnormal sub-regions that are incorrectly classified as normal regions.

The Sensitivity, Specificity, and Accuracy are then defined as Equations.(26-28).

$$Sensitivity = \frac{TP}{TP + FN} \quad (26)$$

$$Specificity = \frac{TN}{TN + FP} \quad (27)$$

$$Accuracy = \frac{TP}{TP + FN + TN + FP} \quad (28)$$

For a fair comparison, seven texture features for each method are extracted that we have mentioned before. The methods SGLDM, GLRLM, GLDM and UEM are used for comparing the results with proposed method. Texture features are extracted in four directions: 0, 45, 90, and 135 (for rotate variant methods). The inner distances for SGLDM and GLDM were set to 1; these provided the best result for all methods. For the proposed method, the best result was achieved by setting the number of neighboring pixels at 8 and setting the radius to 1. As these tables (TABLE I, TABLE II, TABLE III, TABLE IV) show, most of the time our proposed method reach to higher accuracy than other methods. These tables compare the accuracies of methods by using SVM.

Considering the Table I, it shows that proposed method has better sensitivity, specificity and accuracy rather than uniformity estimation method (UEM). Both of proposed and UEM methods are rotation invariant. Tables II, III and IV determine the results of nodule detection, using GLDM, SGLDM and GLRLM and compare these results with proposed method. These three methods are not rotate invariant. Therefore in the CT images, first we train SVM classifier by using original CT images, then in test part the rotated CT images are used and texture features are extracted by using rotated images in four directions: 0, 45, 90, and 135. Considering the result of Table II, it illustrates that for all directions the GLDM has worse result than proposed method. Only for GLDM90 the specificity is the same as proposed method. Also the proposed method has better performance than SGLDM for all result values of Table III. In this table only for SGLDM0 the sensitivity is better than proposed method. Table IV show the result of nodule detection for proposed and GLRLM methods. It is simple to show that proposed method has better specificity in most cases but the sensitivity of it, is lower than that of GLRLM. It is because of the greater number of abnormal sub-regions that are incorrectly classified as normal regions in proposed method. Although the proposed method has lower sensitivity in some case, the overall accuracy of it is better than GLRLM in all cases. Furthermore, the proposed method is a rotation invariant method, however in these three methods the result of the process changes when the CT images are rotated. The results of these tables are related to the accuracy of nodule detection using large sub-regions for feature extraction and using in LibSVM. It is possible to use small or large sub-regions for train and test of SVM but using small sub-regions does not change these results significantly.

TABLE I: COMPARING CLASSIFICATION ACCURACY OF UM AND PROPOSED METHOD (BOTH METHODS ARE ROTATE INVARIANT).

Method	Sensitivity (%)	Specificity (%)	Accuracy(%)
Proposed	96.40	99.60	98.00
UEM	96.30	98.10	97.20

TABLE II: COMPARING CLASSIFICATION ACCURACY OF GLDM AND PROPOSED METHOD IN FOUR DIRECTIONS.

Method	Sensitivity (%)	Specificity (%)	Accuracy (%)
Proposed	96.40	99.60	98.00
GLDM 0	86.40	98.40	92.40
GLDM 45	92.00	98.50	95.25
GLDM 90	91.40	99.60	95.50
GLDM 135	93.20	98.20	95.70

TABLE III: COMPARING CLASSIFICATION ACCURACY OF SGLDM AND PROPOSED METHOD IN FOUR DIRECTIONS.

Method	Sensitivity (%)	Specificity (%)	Accuracy (%)
Proposed	96.40	99.60	98.00
SGLDM 0	98.00	90.00	94.00
SGLDM 45	92.60	95.40	94.00
SGLDM 90	89.00	98.00	93.50
SGLDM135	88.60	97.80	93.20

TABLE IV: COMPARING CLASSIFICATION ACCURACY OF GLRLDM AND PROPOSED METHOD IN FOUR DIRECTIONS.

Method	Sensitivity (%)	Specificity (%)	Accuracy (%)
Proposed	96.40	99.60	98.00
GLRLM 0	97.00	92.00	94.50
GLRLM 45	98.00	84.00	91.00
GLRLM 90	90.20	99.80	95.00
GLRLM 135	98.60	78.40	88.50

After nodule detection, the proposed nodule segmentation is applied to detected sub-regions and volumes of the detected nodules are calculated. Nodules can be divided into three categories, small (diameter<8mm), medium and large (diameter >12mm). In TABLE V and TABLE VI the result of the measurement of nodules are compared with grand truth values. Grand truth values of nodules were determined by three specialists. The accuracy of calculated volume can be obtained as Equation (29)

$$Accuracy = \left(1 - \frac{|V_r - V_m|}{V_r}\right) * 100 \quad (29)$$

Where V_r is real volume of each nodule that is determined by specialists and V_m is measured volume by using proposed method. TABLE V shows the results of using small sub-region for texture extraction and test and train by SVM and TABLE VI determines the same results with large sub-regions. Using large sub-region reduces computational complexity. But if the large sub-regions are used, the volume measurement accuracy will decrease slightly. By using proposed threshold method, more accurate results are produced. The proposed method extracted nodule from its background by using threshold that is calculated based on texture information of nodule. This method is compared with threshold methods of Otsu and threshold method that uses histogram. This means nodule is extracted from background of detected sub-region by using proposed method to remove vessels and any similar intensity part of background then a traditional threshold method is used for nodule segmentation. Also by using Otsu and histogram threshold method nodule is extracted from its background. Table V and VI compare the results of these methods and method for small and large sub-region. These tables show the better accuracy for small and large nodules for proposed method. But the result of proposed method for small sub-regions is better than other two methods significantly. Considering the results, these tables show that using large sub-regions which decreases the accuracy of volumetric. Also using proposed method with suitable T such as T = 20 produces good measurement accuracy. If T is large the fewer vessels parts are excluded and vice versa. It means that if T is very small some parts of nodule may be deleted as a vessel. Increasing the T value has a limit and after that, it has not significant effect on image. Also, as it can be visited from Fig.13, using proposed method removes vessel part and reduces the error of nodule volumetric (False positive reduction for nodule segmentation). Fig.13.b shows an example of performance of proposed method. Considering this figure, it shows the importance of using TLBP method to extract nodule part from its background. Whereas in Fig.13.a a vessel that is connected to nodule (indicated by a circle) is extracted as a nodule part.

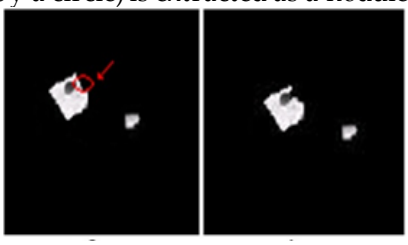

(a) (b)

Fig. 13: Extraction nodule parts from their background, a) Histogram threshold; b) proposed threshold.

Tables V and VI show the results of volumetric for small and large sub-regions respectively. Table V illustrates that the accuracies of volumetric for TLBP method are better than both Otsu and Histogram method. It means if TLBP method is used for nodule segmentation then volume of segmented nodule is calculated the result of volumetric is better than using Otsu or histogram method for nodule segmentation. The best T value in TLBP is related to difference of the intensity of vessel and nodule part in GLELBP image (not in the original image). If T is very small some parts of nodule may be deleted such as Fig.12.a and if it is too large some vessels may be segmented as a nodule part. Both of these decrease the accuracy of volumetric. Table VI is the same as Table V, but it demonstrates the result of methods for large sub-regions. Using larger sub-regions increases the error of volumetric slightly. However it increases computational complexity because of the more number of samples in train and test steps in SVM. Some visual examples of proposed method are shown in Fig.14. Row (a) represents the original CT images, row (b) shows extracted lung from CT images and (c) indicates segmented nodules.

TABLE V: COMPARING THE ACCURACIES OF VOLUME MEASURMENTS USING PROPOSED METHOD AND OUSO AND HISTOGRAM THRESHOLD METHODS (FOR SMALL SUB-REGION)

Method	Small Nodule(%)	Medium Nodule(%)	Large Nodule(%)
TLBP Mask (T=10)	75.45	84.55	92.05
TLBP Mask (T=20)	77.95	85.20	94.65
TLBP Mask (T=40)	77.40	85.10	94.70
Otsu Method	71.60	82.80	91.20
Histogram Method	68.65	73.10	91.00

TABLE VI: COMPARING THE ACCURACIES OF VOLUME MEASURMENTS USING PROPOSED METHOD AND OUSO AND HISTOGRAM THRESHOLD METHODS (FOR LARGE SUB-REGION)

Method	Small Nodule (%)	Medium Nodule (%)	Large Nodule (%)
TLBP Mask (T=10)	75.25	84.40	91.35
TLBP Mask (T=20)	77.40	85.20	94.45
TLBP Mask (T=40)	77.20	85.00	94.55
Otsu Method	69.40	81.60	90.80
Histogram Method	65.65	70.40	90.90

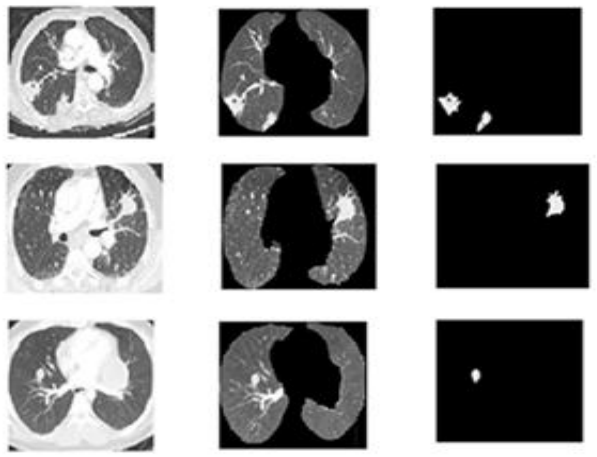

(a) (b) (c)

Fig. 14: a) Original images; b) Segmented lungs; c) Detected nodules

4. CONCLUSION

In this paper, an automatic method is proposed that detect lung nodule in CT images. The proposed method consists of three steps; 1) preprocessing and lung segmentation 2) feature extraction and 3) nodule detection (Classification) at the beginning of the process some enhancement methods are used to improve quality of image. Then a concavity degree method is used which can extract lung areas from the CT image. In this paper a version of local binary pattern is proposed to extract texture feature of nodules and using them for each sub-region of image. This method is robust to noise and correct noise effects by using uniform and symmetrical information of local patterns. Extracted features are used in a SVM classifier to detect sub-regions that contain nodule. After detection of each sub-region of nodule, a new method of thresholding is proposed that is used for nodule segmentation which can extract nodule part from its background such as vessels that have the intensity similar to gray level of nodules and it is not possible to distinct between nodule and this type of background by using traditional threshold. The proposed method is based on the texture information which can mask vessel parts of image and extract contour of each nodule efficiently. Finally, by calculating the area of each segmented nodule and using the thickness of CT slices the volume of each nodule is calculated and this volume is compared with result that is prepared by some specialists. One of the drawback of our methods is related to very small nodule (diameter<5mm). In this paper and in most previous researches, it is not possible to detect this type of nodule so one of the next works that can be extended in future is related to automatic detection of very small nodules.

ACKNOWLEDGMENT

The authors would like to thank Mr. Stelmo Magalhaes Barros Netto for providing volume information about CT data used in this manuscript. They also would like to thank TABA medical imaging center of Shiraz medical school for providing real CT data.

REFERENCES

[1] T.K. Liang, T. Tanaka, H. Nakamura, A. Ishizaka, A neural network based computer-aided diagnosis of emphysema using CT lung images, in: Proceedings of the SICE Annual Conference, Kagawa University, Takamatsu City, Japan, September 1720, pp. 703709 (2007).

[2] B. Sahiner, H.-P.Chan, L.M.Hadjiiski, P.N. Cascade, E.A.Kazerooni, A.R.Chughtai, C. Poopat, T.Song, L.Frank, J.Stojanovska, A.Attili, Effect of CAD on Radiologists detection of lung nodules on thoracic CT scans : analysis of an observer performance study by nodule size, Acad. Radiol.y16(12)(2009).

[3] R.Yuan, P.M.Vos, P.L.Cooperberg, Computer-aided detection in screening CT for pulmonary nodules, Am.J.Roentgenol.186(5), (2006).

[4] K.Marten, C.Engelke, Computer-aided detection and automated CT volumetry of pulmonary nodules,Eur.Radiol.17(2007).

[5] Asem M. Ali, Ayman S. El-Baz, Aly A. Farag, A Novel framework for accurance lung segmentation using graph cuts, in Proc. of ISBI 2007, pp. 908 – 911.

[6] Nisar Ahmed Memon, Anwar Majid Mirza, and S.A.M. Gilani, "Deficiencies of Lung Segmentation Techniques using CT Scan Images for CAD", World Academy of Science, Engineering and Technology 2008 .

[7] M. Keshani, Z. Azimifar and R. Boostani, Lung Nodule Segmentation Using Active Contour Modeling ,6th Iranian Conference on Machine Vision and Image Processing, (2010).

[8] Zhang, X.; McLennan, G.; Hoffman, EA.; Sonka, M. Automated detection of small-size pulmonary nodules based on helical CT images; Proceedings of 19th International Conference on Information Pro cessing in Medical Imaging; Glenwood Springs (USA), (2005).

[9] S. Shimoyama, N. Homma, M. Sakai, T. Ishibashi, and M. Yoshizawa, Auto-detection of non-isolated pulmonary nodules connected to the chest walls in X-ray CT images, in Conf. IEEE ICCAS-SICE, (2009).

[10] H. Zhang, J.E. Fritts, S.A. Goldman, A fast texture feature extraction method for region-based image segmentation, Image and Video Communications and Processing , (2005).

[11] Z. Wang, A. Guerriero, M.D. Sario, Comparison of several approaches for the segmentation of texture images, Pattern Recognition Letters 17 (1996).

[12] Y. Zhang, X.J. He, J.H. Han, Texture feature-based image classification using wavelet package transform, Advances in Intelligent Computing 3644 (2005).

[13] R.W. Conners, C.A Harlow, A theoretical comparison of texture algorithms, IEEE Transactions: Pattern Analysis and Machine Intelligence (1980).

[14] T. Glatard, J. Montagnat, I.E. Magnin, Texture based medical image indexing and retrieval: application to cardiac imaging, in: Proceedings of the Sixth ACM SIGMM International Workshop on Multimedia Information Retrieval, New York, USA, October 1516, (2004).

[15] D.H. Kim, Image recommendation algorithm using feature-based collaborative lettering, IEICE TRANSACTIONS on Information and Systems E92-D , (2009).

[16] A.H. Mir, M. Hanmandlu, S.N. Tandon, Texture analysis of CT images, in: Engineering in Medicine and Biology Magazine, vol.14, IEEE, (1995).

[17] S.Ozekes, Rule based lung region segmentation and nodule detection via genetic algorithm rained template matching, IstanbulCom-mer.Univ.J.Sci.6 (11) (2007).

[18] S.Ozekes, O.Osman, O.N.Ucan, Nodule detection in a lung region that's segmented with using genetic cellular neural networks and 3D template matching with fuzzy rule based thresholding, KoreanJ.Radiol.9(2008).

[19] X.Ye, G.Beddoe, G.Slabaugh, Graph cut-based automatic segmentation of lung nodules using shape, intensity, and spatial features, in: The Second International Workshop on Pulmonary Image Analysis, pp.103113, (2009).

[20] M.Antonelli, G.Frosini, B.Lazzerini, F.Marcelloni, Automated detection of Pulmonary nodules in CT scans, in: International Conference on Computational Intelligence for Modeling, Control and Automation, vol.2,2005,pp.799803.

[21] A.E.-B.G.Gimelfarb, R.F.M.A.El-Ghar, Computer aided characterization of the solitary pulmonary nodule using volumetric and contrast enhancement features, Acad.Rodiol.1213101319, (2005).

[22] T.Messay, R.C.Hardie, S.K.Rogers, A new computationally efficient CAD system for pulmonary nodule detection in CT imagery, Med.ImageAnal.14 (3) 390406, (2010).

[23] M. Tan, R.Deklerck, B.Jansen, M.Bister, J.Cornelis, A novel computer-aided lung nodule detection system for CT images,Med.Phys.38(10)(2011).

[24] R. Opfer, R.Wiemker, Performance analysis for computer-aided lung nodule Detection on LIDC data, in: Proceedings of theSPIE,vol.6515, (2007).

[25] T. Ojala, M. Pietikainen, D. Harwood, A comparative study of texture measures with classication based on feature distributions, Pattern Recognition (1996).

[26] T. Ojala, M. Pietikainen, T. Maenpaa, Multiresolution gray-scale and rotation invariant texture classification with local binary patterns, IEEE Transactions on Pattern Analysis and Machine Intelligence 24 (7) (2002).

[27] Ko JP, Rusinek H, Jacobs EL, et al. Small pulmonary nodules: volume measurement at chest CT Phantom study. Radiology, (2003).

[28] Wormanns D, Kohl G, Klotz E, et al. Volumetric measurements of pulmonary nodules at multi-row detector CT: in vivo reproducibility. EurRadiol, (2004).

[29] Marten K, Rummeny EJ, Engelke C. Computer-aided diagnosis and vol-umetry of pulmonary nodules: current concepts and future perspectives. For tschrRoentgenstr, (2005).

[30] Yankelevitz DF, Reeves AP, KostisWJ,Zhao B, Henschke CI Small pulmonary nodules: volumetrically determined growth rates based on CT evaluation. Radiology 217:251256, (2000).

[31] Yankelevitz DF, Gupta R, Zhao B, Henschke CI Small pulmonary nodules: evaluation with repeat CT preliminary experience. Radiology 212:561566, (1999).

[32] Winer-Muram HT, Jennings SG, Tarver RD et al. Volumetric growth rate of stage I lung cancer prior to treatment: serial CT scanning. Radiology 223:798805, (2002).

[33] Wormanns D, Diederich S, Lentschig MG, Winter F, Heindel W Spiral CT of pulmonary nodules: inter-observer variation in assessment of lesion size. EurRadiol 10:710713, (2000).

[34] Eisenhauer E.A., Therasse P., Bogaerts, J., et al., "New response evaluation criteria in solid tumors': revised RECIST guideline (version 1.1)". Eur J Cancer, 45 (2), 228-47 (2009).

[35] Therasse P., Arbuck S.G., Eisenhauer E.A., et al., "New guidelines to evaluate the response to treatment in solid tumors. European Organization for Research and Treatment of Cancer, National Cancer Institute of the United States, National Cancer Institute of Canada" .J Natl Cancer Inst, 92 (3), 205-16 (2000).

[36] Buckler A.J., Mulshine J.L., Gottlieb, R., et al., "The use of volumetric CT as an imaging biomarker in lung cancer". Acad Radiol, 17 (1), 100-6 (2010).

[37] Gavrielides M.A., Kinnard L.M., Myers K.J., et al., "Non classified lung nodules: volumetric assessment with thoracic CT". Radiology, 251(1), 26-37 (2009).

[38] R. C. Gonzalez, R. E. Woods, Digital Image Processing, Second Edition, Prentice hull (2002).

[39] Nobuyuki Otsu, A Threshold Selection Method From Gray Level Histogram, IEEE Transactions On System, Man And Cybernetics, Vol.9, PP. 62-67, (1979).

[40] Mohammadi Mohammad Reza, Concavity Degree: A New Feature for Chromosome Centromere Localization, ,16th Iranian Conference on Artificial Intelligent and Signal Processing, (2012).

[41] S. Penga, D.Kim, S. Lee , M. Lim, "Texture feature extraction based on a uniformity estimation method for local brightness and structure in chest CT images", Computers in Biology and Medicine 40 ,931942, (2010).

[42] T.K. Liang, T. Tanaka, H. Nakamura, A. Ishizaka, A neural network based computer-aided diagnosis of emphysema using CT lung images, in: Proceedings of the SICE Annual Conference 2007, Kagawa University, Takamatsu City, Japan, September 1720, pp. 703709, (2007).

[43] T. Ahonen, A. Hadid and M. Pietikainen, Face description with local binary patterns: application to face recognition, in: Proceedings of the Eighth European Conference on Computer Vision, vol. 28, pp. 469481, (2004).

[44] G. Tian, H. Fu, D.D. Feng, Automatic medical image categorization and annotation using LBP and MPEG-7 Edge histograms, Proceedings of the Fifth International Conference on Information Technology and Application in Biomedicine, Shenzhen, China, pp. 5153,(2008).

[45] K. Mikolajczyk, C. Schmid, A performance evaluation of local descriptors, IEEE Transactions on Pattern Analysis and Machine Intelligence 27, 16151630, (2005).

[46] D.G. Lowe, Distinctive image features from scale-invariant key point, Computer Vision 2, (2004).

[47] B. Park, Y.R. Chen, Co-occurrence matrix texture features of multi-spectral images on poultry carcasses, Journal of Agricultural Engineering Research Volume 78 (2) 127139, (2001).

[48] W.E. Lorensen and H.E. Cline, Marching Cubes: a high resolution 3D surface construction algorithm, Computer Graphics, Vol. 21, No. 4, pp 163-169 (Proc. of SIGGRAPH), (1987).

[49] https://wiki.cancerimagingarchive.net/display/Public/LIDC-IDRI

[50] www.csie.ntu.edu.tw/cjlin/libSvm.